Examination of near-wall hemodynamic parameters in the renal bridging stent of various stent graft configurations for repairing visceral branched aortic aneurysms

Taylor Suess, MS,[a] Joseph Anderson, BS,[b] Laura Danielson, MD,[b] Katie Pohlson, BS,[b] Tyler Remund, PhD,[b] Elizabeth Blears, MD,[b] Stephen Gent, PhD,[a] and **Patrick Kelly, MD,[b]** *Brookings and Sioux Falls, SDak*

Objective: **This study examined the flow behavior of four stent graft configurations for endovascular repair of complex aneurysms of the descending aorta.**
Methods: **Computational fluid dynamics models with transient boundary conditions and rigid wall simplifying assumptions were developed and used with four distinct geometries to compare various near-wall hemodynamic parameters.**
Results: **Graphic plots for time-averaged wall shear stress, oscillating shear index, and relative residence time were presented and compared among the four stent graft configurations of interest.**
Conclusions: **Abrupt 90° and 180° changes in stent geometry (particularly in the side branches) cause a high momentum change and thus increased flow separation and mixing, which has significant implications in blood flow characteristics near the wall. By comparison, longer bridging stents provide more gradual changes in momentum, thus allowing blood flow to develop before reaching the target vessel. (J Vasc Surg 2016;64:788-96.)**

Clinical Relevance: **Renal vessel patency is a well-known but rarely talked about challenge with complex aneurysm repair. Many factors need to be optimized to ensure branch vessel patency in aneurysms of the visceral segment, including bridging stent compliance transition, bridging stent material selection and design, and main body graft alignment. One topic that has not been discussed much is the flow characteristics entering the branch. Here we propose a technique to evaluate device configurations and their associated flows for their ability to maintain branch vessel patency.**

The endovascular repair of complex aortic aneurysms requires the inclusion of the visceral branch vessels (celiac, superior mesenteric, and the renal arteries) in the repair. However, the inclusion of these outflow branches has not been without significant challenges. With both thoracic and abdominal aortic aneurysm repair, the outflow portions of the stent grafts are wide and have high flow areas, so they tend to remain patent in most cases.[1] The celiac artery is a large-diameter vessel allowing it to remain patent more often. The superior mesenteric artery (SMA) is not consistently as large in diameter, but faces downward, thus requiring less of a directional change in momentum. The renal arteries, though, are relatively small-diameter vessels that are largely perpendicular to the axis of the aorta and are short in length. This leaves the renal arteries somewhat prone to atherosclerotic formation. Several geometric configurations have been developed to repair aneurysms of the branched segment of the aorta.

The focus of the present study compares the computational fluid dynamics (CFD) results of four endovascular stent graft configurations, including fenestrated,[2] two types of branched,[3,4] and manifold,[5] to determine which design features lend themselves to promoting proper blood flow, particularly to the renal arteries. This study took a particularly close look at the various near-wall hemodynamic (NWH) parameters that have been shown to have an effect on atherosclerotic formation. The focus was on the renal bridging stents, especially the distal end where the stent grafts terminate and transition to native arterial tissue.

Abnormally low values of wall shear stress (WSS) can result in physiological conditions that encourage intimal hyperplasia and thrombus formation. For instance, low levels of WSS may delay nutrient renewal and waste product removal.[6-8] Low WSS can also cause formed elements, such as monocytes, thrombocytes, and granulocytes, to move to peripheral portions of the arterial flow. This may affect the net balance of intimal entry and exit of

From the Department of Mechanical Engineering, South Dakota State University, Brookings[a]; and the Sanford Health, Sioux Falls.[b]
Author conflict of interest: P.K. is an inventor of one of the stent grafts analyzed in this report and has assigned his intellectual property to his employer, Sanford Health. Sanford Health has entered into a licensing agreement with a medical device manufacturer. T.R. and K.P. are also employed by Sanford Health, and all three authors could receive royalties from the agreement.
Correspondence: Patrick Kelly, MD, Sanford Health, 1305 W 18th St, Rte 6133, Sioux Falls, SD 57117 (e-mail: patrick.kelly@sanfordhealth.org).
The editors and reviewers of this article have no relevant financial relationships to disclose per the JVS policy that requires reviewers to decline review of any manuscript for which they may have a conflict of interest.
0741-5214

http://dx.doi.org/10.1016/j.jvs.2015.04.421

monocytes.[9-13] The WSS can be quantified over the entire cardiac cycle by making use of the time-averaged WSS (TAWSS). TAWSS values of <0.4 Pa have been shown to be atherogenic.[7] Regions of unidirectional, moderate shear levels result in elongated and aligned endothelial cells, which form tight intracellular junctions.[14] Deviations from this condition can be problematic.

The oscillating shear index (OSI) has been developed to characterize these areas of varying shear direction. Areas of elevated OSI have been theorized to be leaky to atherogenic particles. OSI values of >0.3 have been shown to be atherogenic.[15]

Relative residence time (RRT) is a theoretical parameter that is intended to indirectly characterize the amount of time atherogenic particles may be in contact with the vessel wall. The longer that atherogenic particles are in contact with the endothelium, the greater chance that they may infiltrate the vascular tissue. It factors in both the TAWSS and OSI. RRT values >10 m^2/N have been shown to promote atherogenic activity[16] (Table).

Table. Reported ranges of near-wall hemodynamic (NWH) parameters that are problematic as reported in the literature

Parameter	*Atherosclerosis-promoting range*
TWSS	<0.4 Pa
OSI	>0.3
RRT	>10 m^2/N

OSI, Oscillating shear index; *RRT*, relative residence time; *TWSS*, time-averaged wall shear stress.

METHODS

The aortic components were all made to have a proximal diameter of 40 mm. The ostium of the SMA was located 20 mm above the ostia of the renal arteries. The ostium of the celiac was 15 mm above SMA, at a 30° rotational offset from the SMA. The seal zone diameters were 8 mm for the celiac, 7 mm for the SMA, 6 mm for the renals, and 16 mm for the iliacs (Fig 1).

In these simulations, we determined that the flow would be developing as it entered the graft; therefore, a particular entrance length was added to the top of each graft to create a partially developed velocity profile in the entering region. The entrance length used was 0.2 m. This was selected because it would provide for a partially developed flow entering the visceral segment, which would be consistent with the actual descending aorta. The outlets were assigned a flow-split outlet boundary condition in which they each call for a specific fraction of the total flow throughout the cardiac cycle. The amount of flow drawn by each outlet was established based on a review of past experimental research.[17] Values for each of the flow fractions were selected for a person who had been fasting and was at rest.

The simulations were performed with the waveforms presented in Fig 2. The supraceliac aortic flow was divided with ~21% of the volume flow of blood going to the celiac, 16% going to the SMA, 15% going to each renal, and 33% going to the infrarenal aorta.[18,19] The supraceliac, SMA, and iliac waveforms were triphasic. The celiac and renal arteries had a more monophasic shape due to their low resistance states at rest.

The flow for the simulation was considered static, three-dimensional, incompressible, and laminar (peak Re = 1250). However, because of the sharp momentum changes from the bifurcations disturbing the flow, we determined that there these simulations would be best modeled with an induced, low Reynolds number, turbulence model. The walls were modeled as nondeforming,[20] and a zero-velocity boundary condition was adopted at the fluid-wall interface, corresponding to a no-slip condition.

The blood flow was also assumed to have an average volumetric flow of 3.8 L/min through the aorta over the entire cardiac cycle, with a peak flow rate of ~9 L/min.[20] Being that non-Newtonian effects are only applicable in vessels <1 mm diameter and our smallest vessel was 6 mm in diameter, we assumed blood was Newtonian with a dynamic viscosity of 0.004 Pa-s and a density of 1050 kg/m^3.

To minimize surface roughness effects to isolate the effect of the stent graft configuration on NWHs, the walls were modeled as smooth, rigid, and nondeforming. The NWH parameters TAWSS and OSI have been shown to be accurate in rigid wall models of the aorta.

The models of the various grafts were created in Creo 2.0 computer-assisted design software (PTC Inc, Needham, Mass) and transferred to Star-CCM+ 9.04 CFD software (CD-Adapco, Melville, NY). Here, the three-dimensional computer-assisted design models were meshed and defined for analysis. An initial mesh refinement study was performed to analyze the effect that the number of cells has on the accuracy, or mesh convergence, of the simulation. The mesh size was gradually reduced for various iterations and tested at several refinement points for increases in accuracy of the simulations. Minimal improvements were noted by further refinement with the mesh containing a base target cell size of 1 mm and a base minimum cell size of 0.25 mm.

For further validation, past studies of other CFD models of various parts of the vascular system were analyzed for their cell size.[21-24] For each of these studies, individual mesh refinement studies resulted in maximum cell sizes between 0.5 and 1.5 mm, generating varying amounts of cells based on the region of the vascular system modeled. One of these studies[22] achieved velocity convergence in all low-to-medium turbulence areas within this range of cell sizes; thus, a cell size range from 0.25 mm to 1 mm was deemed appropriate for this study. To acquire the same degree of accuracy for all simulations, the same base cell sizes were used for each graft, which also assured proper simulation convergence. A polyhedral mesher was used for the internal fluid cells, because this cell type enables the level of model refinement required for this study

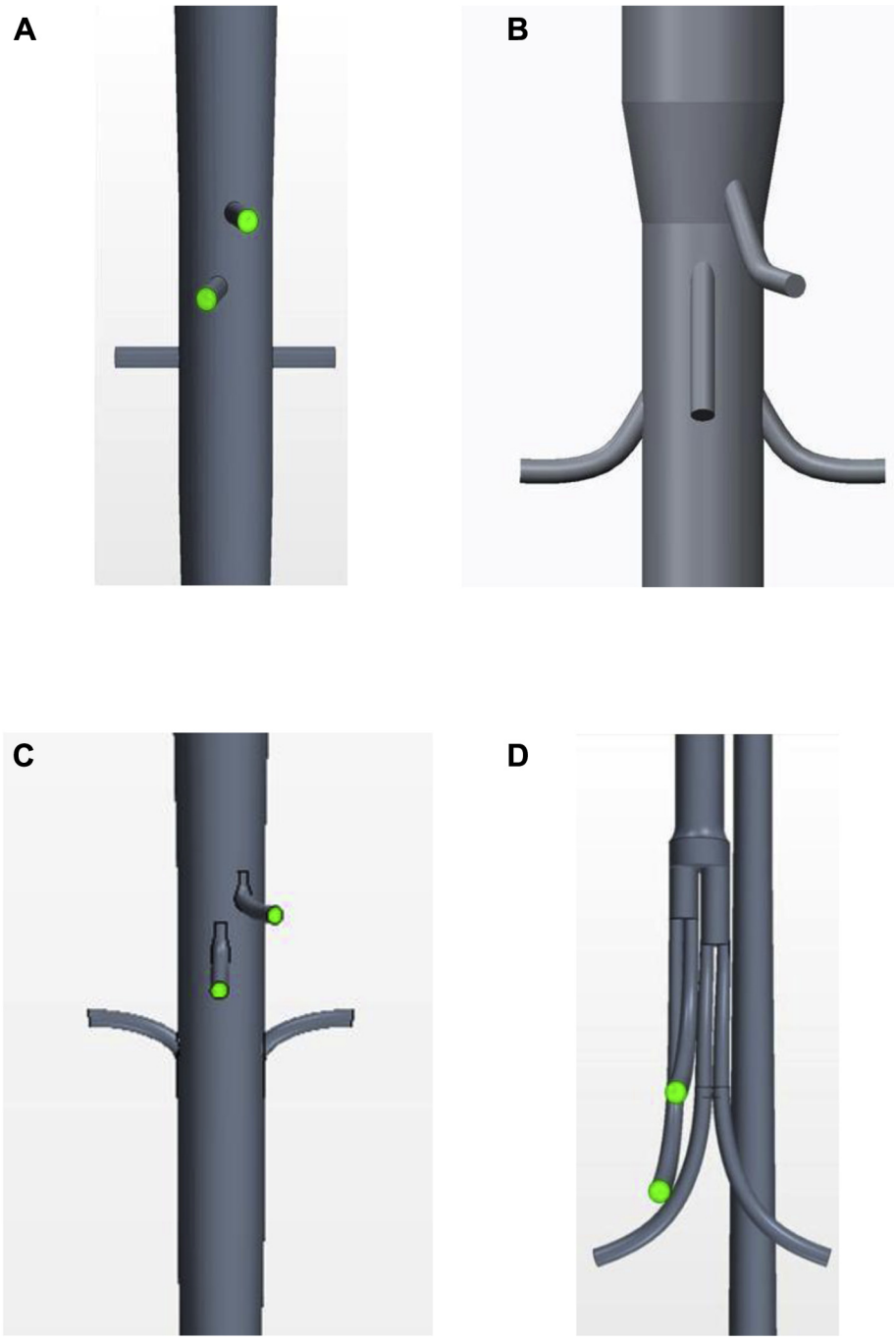

Fig 1. An anterior view is shown of the geometries of each of the graft configurations: **(A)** fenestrated, **(B)** antegrade branched, **(C)** retrograde branched, and **(D)** manifold stent graft.

while minimizing convergence time and required computing capacity. In addition, an advancing layer mesher was added to create prism layers near the boundaries for additional refinement. These extremely thin layers of cells provide increased robustness of near-wall conditions, especially WSS values. By inserting 20 prism layers, these meshes would be able to capture these important boundary layer flows and wall parameters accurately. The combination of these meshing schemes and the base cell sizes listed resulted in cell numbers of each simulation ranging from 1,801,495 cells (fenestrated) to 3,091,452 cells (manifold), based on overall graft complexity and total graft volume.

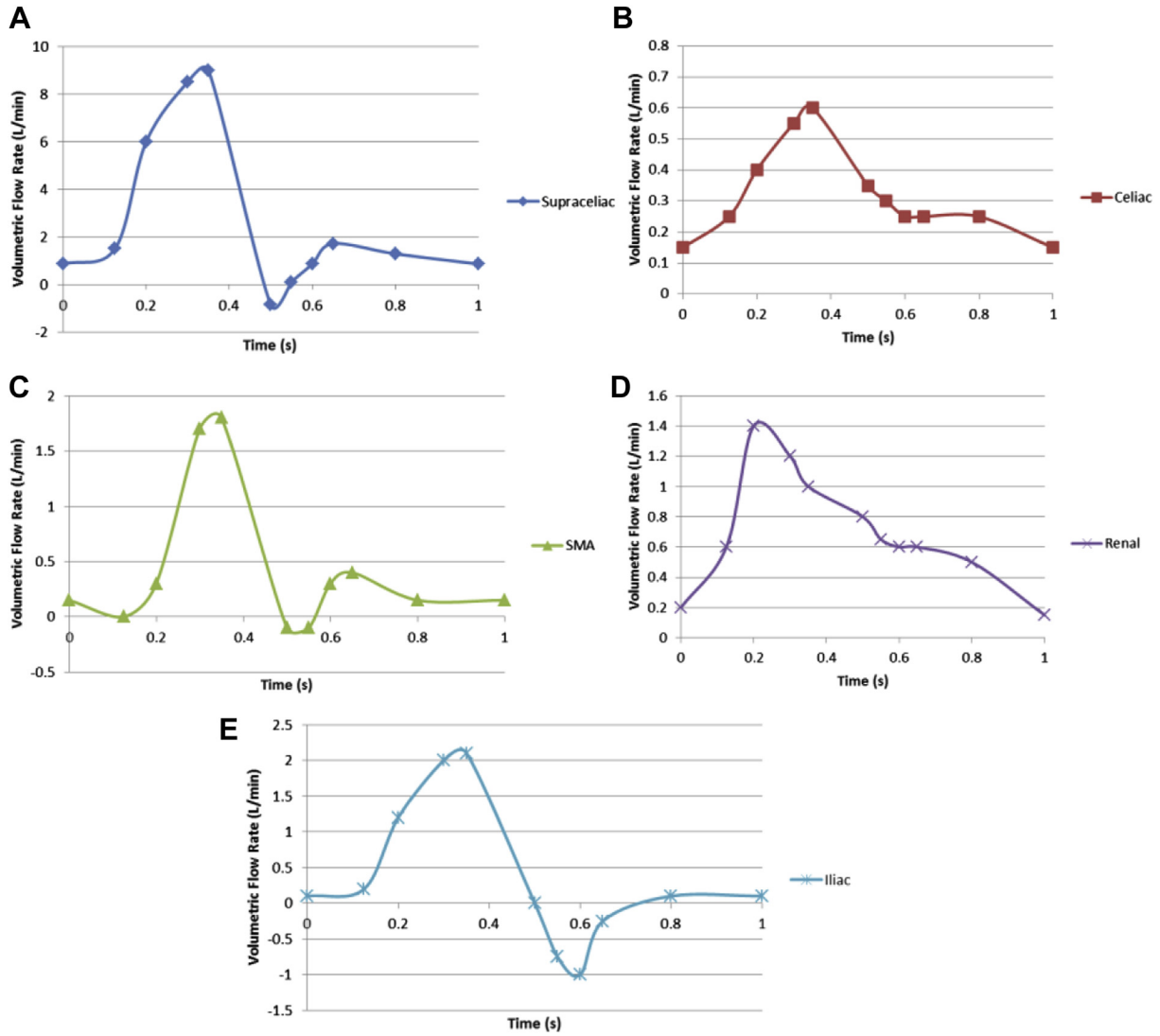

Fig 2. Volume flow rates (L/min) of the **(A)** supraceliac aorta, **(B)** celiac artery, **(C)** superior mesenteric artery (*SMA*), **(D)** renal arteries, and **(E)** iliac arteries.

A transient flow model was used to generate a TAWSS map for each of the four stent graft configurations. TAWSS is the integration of each nodal WSS magnitude over the cardiac cycle. TAWSS is defined in Equation 1.

$$\text{TAWSS} = \frac{1}{T}\int_0^T |\tau_w| dt \tag{1}$$

T = Time of the cardiac cycle [s]; t = time[s]; τ_w = WSS (Pa)

The OSI is a dimensionless metric of changes in WSS direction.[25] OSI is a time-dependent quantity defined using Equation 2.

$$OSI = \text{oscillating shear index} = 0.5\left(1 - \frac{\left|\int_0^T \vec{\tau}_w dt\right|}{\int_0^T \left|\vec{\tau}_w\right| dt}\right) \tag{2}$$

T = Time of the cardiac cycle (s)]; $\vec{\tau}_w$ = the WSS vector [Pa]; t = specific time point of the cardiac cycle [s]

The RRT is inversely proportional to both TAWSS and OSI. RRT can be calculated from Equation 3.

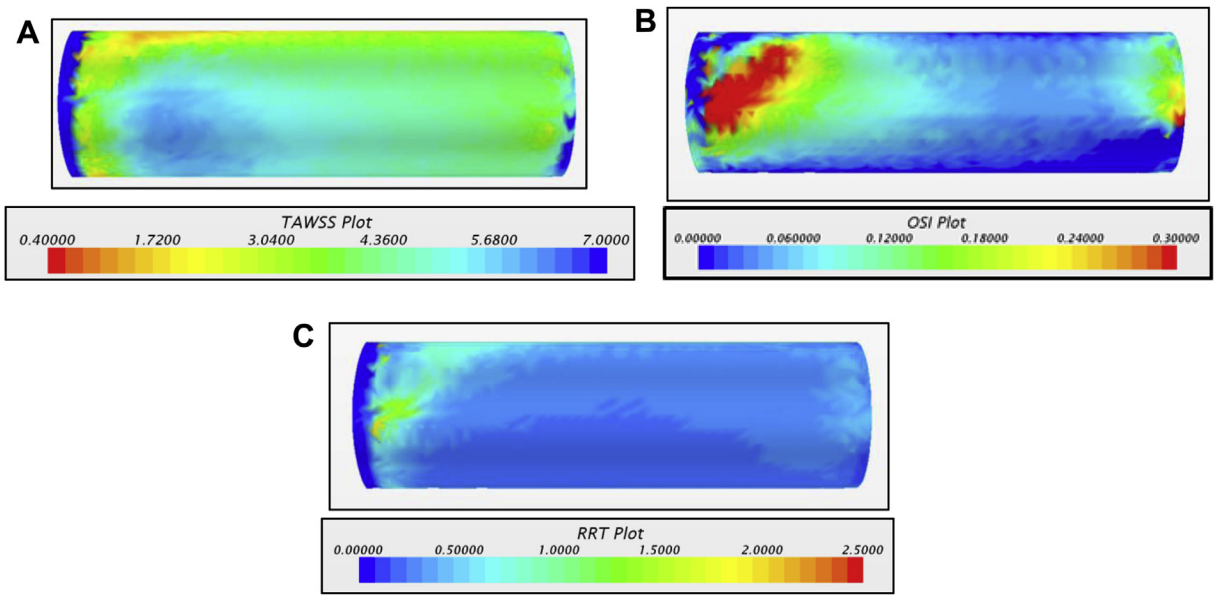

Fig 3. Near-wall hemodynamic (NWH) parameters for the renal vessel of the fenestrated configuration, including **(A)** time-averaged wall shear stress (*TAWSS*; Pa), **(B)** oscillating shear index (*OSI*; s/s), and **(C)** relative residence time (*RRT*; N/m^2).

$$\mathrm{RRT} = \frac{1}{(1 - 2 * OSI) * TAWSS} \tag{3}$$

OSI = Oscillating shear index [unitless]; TAWSS = time-averaged wall shear stress [Pa]

RESULTS

The proposed CFD simulations were completed for each graft configuration. Presented here are various parameters measured, including transient simulations with analyses showing the various NWH parameters, including TAWSS, OSI, and RRT.

The results from the simulation of the fenestrated configuration are shown with a focus on the renal bridging stent grafts in Fig 3. Fig 3, *A* shows the TAWSS for the fenestrated configuration. There appears to be a moderate amount of TAWSS along the entire length of the bridging stent graft, including the distal portion. Fig 3, *B* shows the OSI in the bridging stent graft for the fenestrated configuration. There appears to be a region of significantly elevated OSI along the proximal extent. Finally, the RRT for the fenestrated configuration is shown in Fig 3, *C*. It appears that there is only a small region of slightly elevated RRT on the proximal extent corresponding to the region of elevated OSI in Fig 3, *B*.

The antegrade renal bridging stent graft is shown in Fig 4. The TAWSS for the antegrade branch renal bridging stent graft shows elevated values on the proximal end and more moderate values on the distal end (Fig 4, *A*). It then has low levels of OSI on the proximal end and moderate values on the distal end (Fig 4, *B*). Finally, it has low values of RRT on the proximal end and more moderate levels on the distal end of the renal bridging stent (Fig 4, *C*).

The data for the renal bridging stent grafts for the retrograde branch configuration are shown in Fig 5. The TAWSS is shown in Fig 5, *A*, and it appears that the bridging stent graft has elevated TAWSS along the proximal lateral portion and distal cranial portion. It also shows relatively low TAWSS values along the proximal medial portion and distal caudal portion of the renal bridging stent graft. In Fig 5, *B* it appears that the renal bridging stent graft has elevated the OSI values at the proximal and distal extent of the bridging stent graft. Finally, in Fig 5, *C* it appears that the renal bridging stent has moderate RRT values along the entire length.

The results for the manifold configuration are shown in Fig 6. The TAWSS is low on the proximal end and moderate on the distal end of the renal bridging stent graft (Fig 6, *A*). The OSI values are low throughout the length of the manifold bridging stent graft (Fig 6, *B*). Finally, the RRT is moderate on the proximal end corresponding to the low TAWSS region, and the distal end of the manifold bridging stent graft has a low value for RRT (Fig 6, *C*).

DISCUSSION

The fenestrated branch had consistently moderate values for TAWSS along its length. The configuration has an inlet that requires a 90° change of direction of the momentum of flow, which results in a separation and subsequent flow disturbance. It showed downward flow in the proximal extent of the renal vessel, which resulted in a recirculation zone on the proximal cranial surface of the renal vessel. This shows with an elevated OSI reading on the proximal end (Fig 3, *B*). Although this segment is

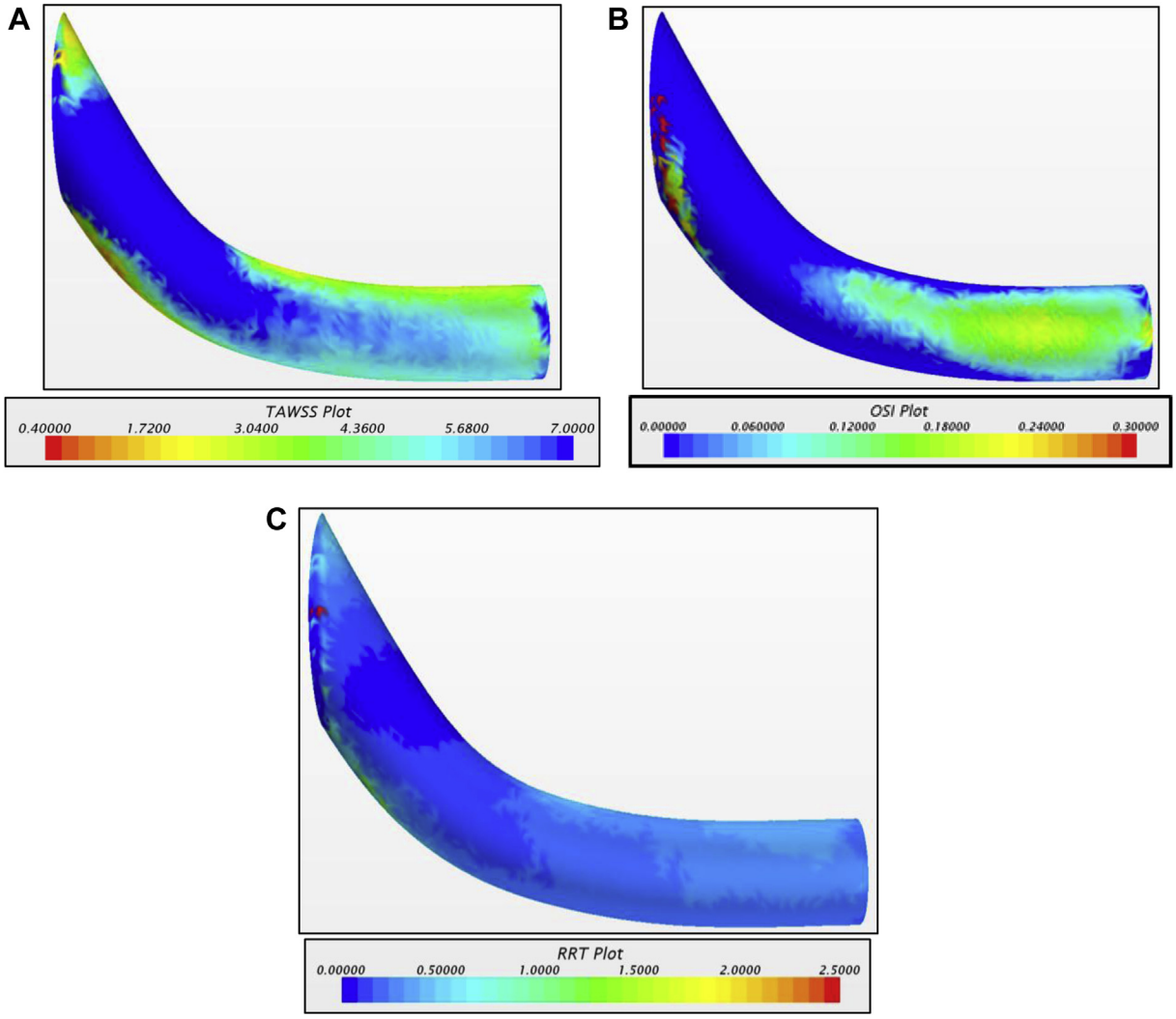

Fig 4. Near-wall hemodynamic (NWH) parameters for the renal vessel of the antegrade branch configuration, including **(A)** time-averaged wall shear stress (*TAWSS*; Pa), **(B)** oscillating shear index (*OSI*; s/s); and **(C)** relative residence time (*RRT*; N/m^2).

covered by the stent if a stent graft is used, many fenestrations use bare metal stents as mating stents, leaving the renal artery exposed to potentially adverse flow conditions. Several real-world conditions that were not accounted for in the model may further exacerbate the issues mentioned in the previous paragraph:

First, the stent struts, in the event bare-metal mating stents are used, will likely result in stagnant zones adjacent to each of the struts until endothelialization is complete.[26]

Second, even though the bare-metal stent is flared around the ostium with a compliant balloon, the proximal extent of the bare-metal mating stent will likely not conform perfectly around the fenestration and will likely extend into the aortic flow channel. This would further add to the disturbed nature of flow in the area.[27]

This effect may be exacerbated by natural respiratory motion. It is speculated that these areas of recirculation are more pronounced momentarily during peak respiratory motion. Peak respiratory motion can reach up to 3-mm displacement both on the proximal and distal end of the renal arteries. However, when a fenestrated graft is implanted, it can reduce the respiratory motion on the proximal end of the renal artery to 25% of its natural displacement and can reduce the motion on the distal end to 80% of its natural displacement.[28] The fixation of the proximal end of the renal bridging stent to the main body component, although allowing relative motion for the distal end, can cause the type of relative stent movement that provokes intimal hyperplasia.

The RRT plot looks mostly favorable for the fenestrated graft, but it appears to have a small location of elevated RRT at the proximal end. Assuming that an elevated RRT corresponds well with areas of particle margination and infiltration, this could result in stenosis

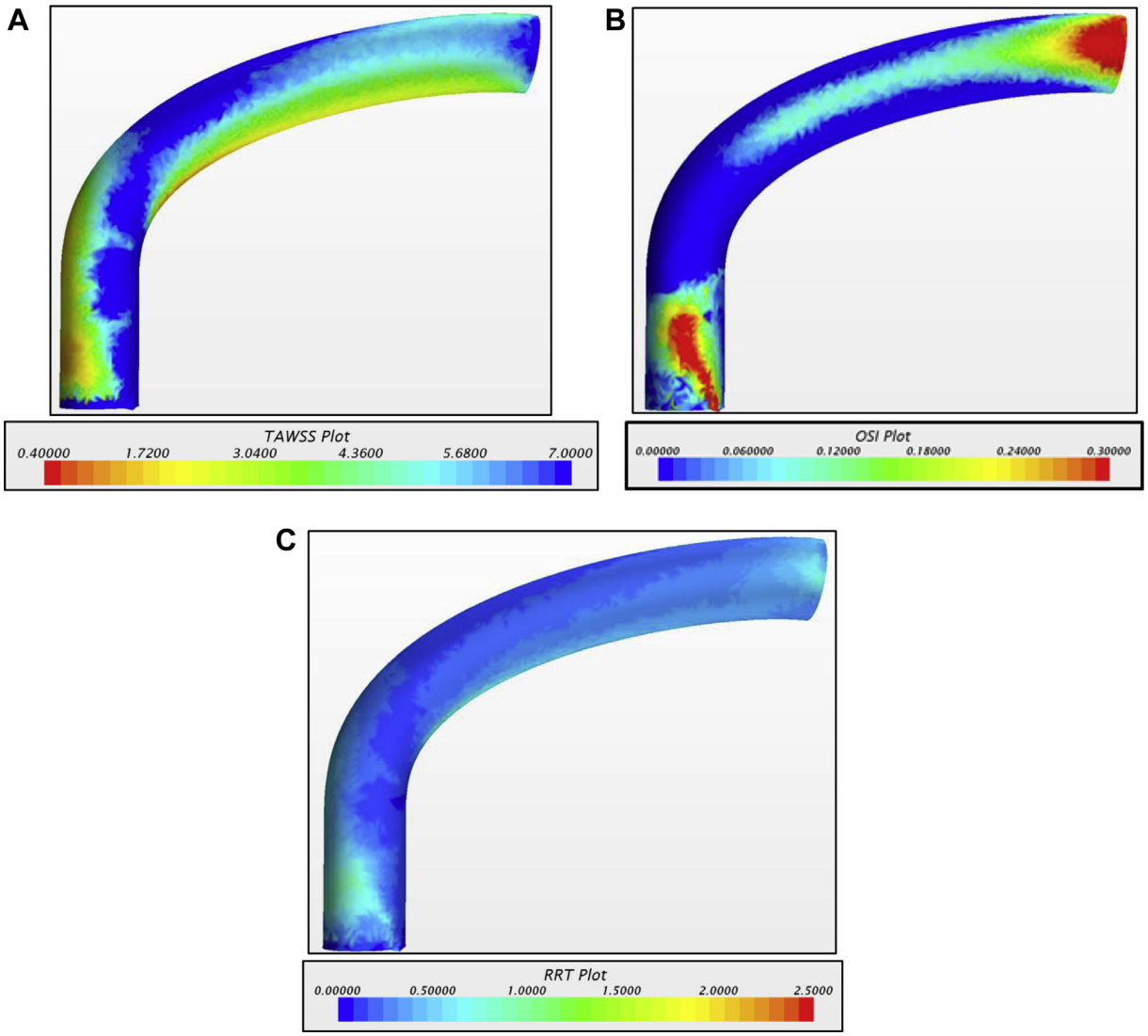

Fig 5. Near-wall hemodynamic (NWH) parameters for the renal vessel of the retrograde branch configuration, including **(A)** time-averaged wall shear stress (*TAWSS*; Pa), **(B)** oscillating shear index (*OSI*; s/s), and **(C)** relative residence time (*RRT*; N/m^2).

of the proximal end of the renal branch, especially because renal ostia tend to have atherosclerotic formation in most people already.

Antegrade branch configurations have an advantage of having all four bridging stent grafts with inlets that have takeoff angles with axes 30° relative to the axis of aortic flow. This decreases flow disturbances in the proximal portions of the renal bridging stent grafts. Although elevated TAWSS levels throughout and the smooth flow in the proximal portion of the renal bridging stent graft where the vessel is covered and oscillations are not exposed to the arterial tissue, the oscillating shear plot showed an increased amount of oscillation on the distal extent of the renal stent graft. The oscillations are only moderate but are on the distal extent of the branch, meaning they are close to being exposed to the arterial tissue. The RRT is not concerning in the antegrade branch stent graft anywhere along its length.

The retrograde branch configuration is a stent graft that allows for preloaded wires in the renal branches, providing ease of cannulation of the renal arteries. However, this advantage of caudally facing bridging stent graft inlets may come at the expense of the quality of flow being delivered the renal arteries. The configuration has a takeoff angle that makes for a 180° turn in the direction of the momentum of blood flow. This creates a condition where there is a greatly disturbed flow at the proximal end of the bridging stent graft. The high shear appears to oscillate from inner to outer curvature surfaces, leaving large regions of the renal vessels open to recirculation and oscillating flows. The

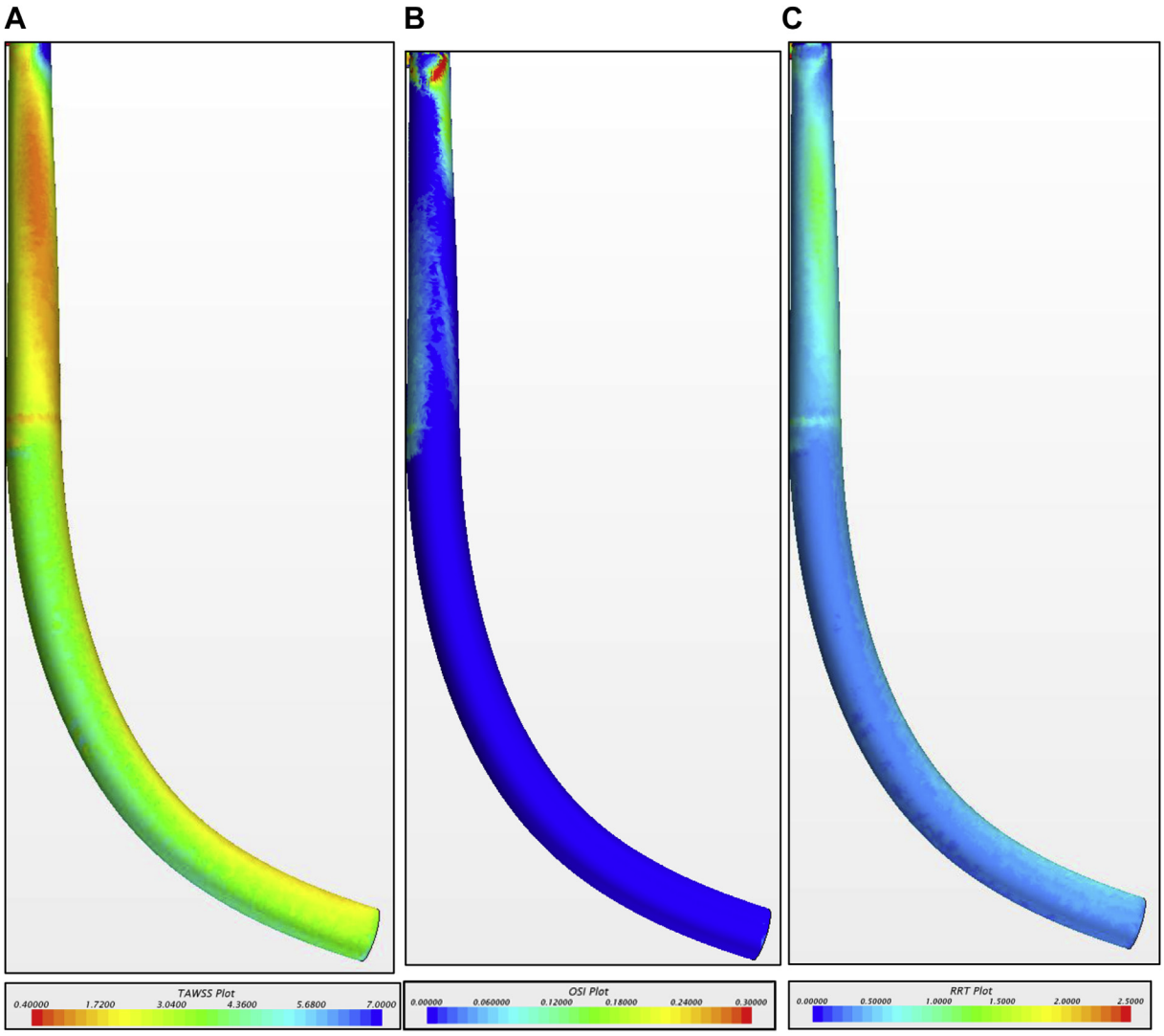

Fig 6. Near-wall hemodynamic (NWH) parameters for the renal vessel of the manifold configuration, including **(A)** time-averaged wall shear stress (*TWSS*; Pa), **(B)** oscillating shear index (*OSI*; s/s), and **(C)** relative residence time (*RRT*; N/m^2).

retrograde renal branch also appears to have a significant peak on the proximal and distal extents of the renal vessel in the OSI plots. The distal peak is most concerning, because it is still increasing as it reaches the uncovered segment where the flow is exposed to the native arterial tissue. This could create an environment prone to intimal trauma and atherosclerotic formation at the transition from covered to uncovered vessel. As expected, the RRT is slightly increased at the proximal and distal extent of the renal bridging stent graft corresponding to the areas where the OSI is elevated.

The manifold inlet receives antegrade flow, and the bridging stent graft take-off angle is tangential to the direction of aortic flow, similar to the antegrade branch. This effectively minimizes separations from momentum direction changes and subsequently minimizes any resulting flow disturbances. The TAWSS appears to be moderate along the length and so is not concerning. The average OSI for the manifold was quite low and dropped off almost immediately after the bifurcation, remaining low throughout the length of the bridging stent grafts. It was interesting that the manifold had very consistent values for RRT along the length of the bridging stent graft. This relatively consistent flow may not be immediately apparent, because proper open surgical technique calls for shorter bypass grafts to be used when possible. However, open bypass grafts can be several orders of magnitude longer than a renal bridging stent. The longer-length bridging stents in the manifold allow for larger radii of curvature in the bridging stents and a longer length along which the flow can develop. The larger radius of curvature prevents the types of drastic flow disturbances that result from sharper turns in momentum.

We note here that these analyses are theoretical in nature because the surfaces were assumed to be smooth and rigid. Smooth surfaces are not the norm in the in vivo environment where the stent graft cloth oscillates with the pulsatility of the flow, patients have varying anatomy where kidney position oscillates with respiration, and where areas of vessel curvature and stenoses may result in areas of recirculation and stagnation causing areas of substantial localized decreases in TAWSS and increases in OSI and RRT. These variations may have effects on the NWH parameters are additive, putting specific patients at elevated risk of restenosis.

CONCLUSIONS

We have presented three NWH parameters that can be used to analyze and potentially enhance stent graft design for complex aneurysm repairs. By using the near-wall analysis and focusing on the distal end of the bridging stent grafts where the stent terminates and flow begins to be exposed to the native arterial tissue, stent grafts can be designed in a way that flows in this area are developed and ordered. This is one of several factors that may contribute to the durability of these repairs.

AUTHOR CONTRIBUTIONS

Conception and design: TS, TR, SG, PK
Analysis and interpretation: TS, TR, SG, PK
Data collection: TS
Writing the article: TS, JA, LD, KP, TR, EB, SG, PK
Critical revision of the article: TS, JA, LD, KP, TR, EB, SG, PK
Final approval of the article: PK
Statistical analysis: Not applicable
Obtained funding: Not applicable
Overall responsibility: PK

REFERENCES

1. van Keulen JW, de Vries JP, Dekker H, Gonçalves FB, Moll FL, Verhagen HJ, et al. One-year multicenter results of 100 abdominal aortic aneurysm patients treated with the Endurant stent graft. J Vasc Surg 2011;54:609-15.
2. Kitagawa A, Greenberg RK, Eagleton MJ, Mastracci TM. Zenith p-branch standard fenestrated endovascular graft for juxtarenal abdominal aortic aneurysms. J Vasc Surg 2013;58:291-300.
3. Quinn SF. W. L. Gore & Associates, Inc, assignee. Method of deploying bifurcated side-access intravascular stent graft. U.S. Patent No.: US 8556961 B2. Issued October 15, 2013.
4. Sweet MP, Hiramoto JS, Park KH, Reilly LM, Chuter TA. A standardized multi-branched thoracoabdominal stent-graft for endovascular aneurysm repair. J Endovasc Ther 2009;16:359-64.
5. Anderson J, Nykamp M, Danielson L, Remund T, Kelly PW. A novel endovascular debranching technique using physician-assembled endografts for repairing thoracoabdominal aneurysms. J Vasc Surg 2014;60:1177-84.
6. Caro CG, Fitz-Gerald JM, Schroter RC. Arterial wall shear and distribution of early atheroma in man. Nature 1969;223:1159-60.
7. Malek AM, Alper SL, Izumo S. Hemodynamic shear stress and its role in atherosclerosis. JAMA 1999;282:2035-42.
8. Shaaban AM, Duerinckx AJ. Wall shear stress and early atherosclerosis: a review. AJR Am J Roentgenol 2000;174:1657-65.
9. Joris I, Majno G. Inflammatory components of atherosclerosis. In: Weissmann G, Samuelsson B, Paoletti R, editors. Advances in inflammation research. New York: Raven Press; 1979. p. 71-85.
10. Schaffner T, Taylor K, Bartucci EJ, Fischer-Dzoga K, Beeson JH, Glagov S, et al. Arterial foam cells exhibit distinctive immunomorphologic and histochemical features of macrophages. Am J Pathol 1980;100:57-80.
11. Jorris I, Zand T, Nunnari JJ, Krolikowski FJ, Majno G. Studies on the pathogenesis of atherosclerosis: Adhesion and emigration of mononuclear cells in the aorta of hypercholesterolemic rats. Am J Pathol 1983;113:341-58.
12. Gerrity RG. The role of the monocyte in atherogenesis: I. Transition of blood-borne monocytes into foam cells in fatty lesions. Am J Pathol 1981;103:181-90.
13. Gerrity RG. The role of the monocyte in atherogenesis II. Migration of foam cells from atherogenic lesions. Am J Pathol 1981;103:191-200.
14. Lewis JC, Taylor RG, Jones ND, St Clair RW, Cornhill JF. Endothelial surface characteristics in pigeon coronary artery atherosclerosis. I. Cellular alterations during the initial stages of dietary cholesterol challenge. Lab Invest 1982;46:123-38.
15. He X, Ku DN. Pulsatile flow in the human left coronary artery bifurcation: average conditions. J Biomech Eng 1996;118:74-82.
16. Morbiducci U, Gallo D, Ponzini R, Massai D, Antiga L, Montevecchi FM, et al. Quantitative analysis of bulk flow in image-based hemodynamic models of the carotid bifurcation: the influence of outflow conditions as test case. Ann Biomed Eng 2010;38:3688-705.
17. Elad D, Einav S. Physical and flow properties of blood. In: Kutz M, editor. Standard handbook of biomedical engineering and design. New York: McGraw Hill; 2004;3.1-3.25.
18. Ku DN, Glagov S, Moore JE Jr, Zarins CK. Flow patterns in the abdominal aorta under simulated postprandial and exercise conditions: an experimental study. J Vasc Surg 1989;9:309-16.
19. Taylor CA, Hughes TJ, Zarins CK. Finite element modeling of three-dimensional pulsatile flow in the abdominal aorta: relevance to atherosclerosis. Ann Biomed Eng 1998;26:975-87.
20. Lantz J, Renner J, Karlsson M. Wall shear stress in a subject-specific human aorta—influence of fluid-structure interaction. Int J Appl Mech 2011;3:759-78.
21. Kung EO, Les AS, Medina F, Wicker RB, McConnell MV, Taylor CA. In vitro validation of finite-element model of AAA hemodynamics incorporating realistic outlet boundary conditions. J Biomech Eng 2011;133:041003.
22. Les AS, Shadden SC, Figueroa CA, Park JM, Tedesco MM, Herfkens RJ, et al. Quantification of hemodynamics in abdominal aortic aneurysms during rest and exercise using magnetic resonance imaging and computational fluid dynamics. Ann Biomed Eng 2010;38:1288-313.
23. Molony DS, Callanan A, Kavanagh EG, Walsh MT, McGloughlin TM. Fluid-structure interaction of a patient-specific abdominal aortic aneurysm treated with an endovascular stent-graft. Biomed Eng Online 2009;8:24.
24. Soulis JV, Fytanidis DK, Papaioannou VC, Styliadis H, Giannoglou GD. Oscillating LDL accumulation in normal human aortic arch—shear dependent endothelium. Hippokratia 2011;15:22-5.
25. Ku DN, Giddens DP, Zarins CK, Glagov S. Pulsatile flow and atherosclerosis in the human carotid bifurcation. Positive correlation between plaque location and low oscillating shear stress. Arteriosclerosis 1985;5:293-302.
26. Duraiswamy N, Schoephoerster RT, Moore JE Jr. Comparison of near-wall hemodynamic parameters in stented artery models. J Biomech Eng 2009;131:061006.
27. Moore R, Hinojosa CA, O'Neill S, Mastracci TM, Cina CS. Fenestrated endovascular grafts for juxtarenal aortic aneurysms: a step by step technical approach. Catheter Cardiovasc Interv 2007;69:554-71.
28. Muhs BE, Vincken KL, Teutelink A, Verhoeven EL, Prokop M, Moll FL, et al. Dynamic cine-computed tomography angiography imaging of standard and fenestrated endografts: differing effects on renal artery motion. Vasc Endovascular Surg 2008;42:25-31.

Submitted Feb 24, 2015; accepted Apr 22, 2015.